ACS ES&T Engineering

pubs.acs.org/estengg

Article

Donnan Dialysis Desalination with a Thermally Recoverable Solute

Hanqing Fan and Ngai Yin Yip*

Cite This: ACS EST Engg. 2022, 2, 2076−2085

Read Online

ACCESS | Metrics & More | Article Recommendations | Supporting Information

ABSTRACT: This study presents a novel desalination technology that couples Donnan dialysis (DD) with thermally-recoverable solutes and utilizes low-grade heat as energy input. In the proposed process, saline feed streams and receiver solutions of concentrated $NH_4HCO_{3(aq)}$ flow stepwise across cation- and anion-exchange membranes. The large transmembrane concentration differences of NH_4^+ and HCO_3^- set up electrochemical potential gradients to drive the uphill transport of Na^+ and Cl^- ions, respectively, from the saline feed into the receiver stream. Warming the two outlet streams using low-temperature thermal sources volatilizes NH_3 and CO_2, thus removing NH_4HCO_3 to yield desalinated product water and concentrated brine. The separated $NH_{3(g)}$ and $CO_{2(g)}$ are then recycled to reconstitute the receiver solution. The concept was first experimentally validated by desalinating brackish water simulated with 100 mM NaCl solutions to freshwater salinities (<17 mM). DD desalination was then demonstrated for larger ranges of feed and receiver concentrations of 100−1000 mM, and the experimental salt removals showed good agreement with theoretical Donnan equilibria (within 5%). The experimental results revealed that the unavoidable permeation of receiver solute co-ions due to imperfect membrane permselectivities is the main factor that prevents the theoretical thermodynamic potential from being reached. Nonetheless, current commercial ion-exchange membranes are sufficient to suppress the undesired co-ion leakage, yielding salt removals adequate for practical desalination. Module-scale analysis quantitatively showed that countercurrent DD operation can obtain higher desalination performance compared to co-current flows, achieving salt removals and water recovery yields as high as 95.5 and 87.5%, respectively. The utilization of low-grade thermal sources, such as waste heat and low-temperature geothermal reservoirs, as the primary energy input to drive the innovative approach opens up opportunities to lower the carbon intensity of desalination.

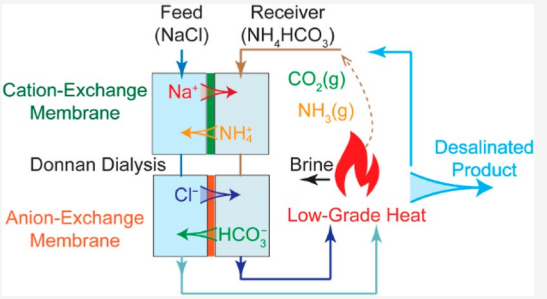

KEYWORDS: *Donnan dialysis, ion-exchange membranes, desalination, low-grade heat*

INTRODUCTION

Providing sustainable access to freshwater is among the grand engineering challenges of the 21st century. Global freshwater scarcity is affecting approximately two-thirds of the world population.[1,2] Meanwhile, population growth, economic development, and climate change exert mounting strains on water security.[1−3] Desalination offers a viable solution to address the growing water supply deficits.[4,5] Salt-water separation processes currently produce ≈95 million m^3/d freshwater from saline streams, such as seawater, brackish water, and wastewater, with continued strong growth projected for the global desalination market.[6] Tapping into the non-freshwater resources through desalination will be indispensable in narrowing the gap between water demand and supply.

The prevailing industrial-scale desalination technologies are thermally driven evaporative processes, for example, multi-stage flash and multiple effect distillation, and electricity-powered membrane processes, for example, reverse osmosis (RO) and electrodialysis (ED).[6] Despite their technical maturity, these conventional desalination methods are still very carbon-intensive.[7−10] Low-temperature heat resources below 100 °C exist in vast amounts, are widely accessible, and can be a low-carbon energy source.[11−13] For example, 43 PW h energy was lost globally as low-grade (<100 °C) waste heat in 2012, from sources such as electricity generation, transportation, the petrochemical industry, and steel production.[11] Geothermal energy is another abundant heat source; in the U.S. alone, ≈14 × 10^6 EJ is estimated to be potentially accessible.[14] However, only a tiny proportion of such low-grade heat is currently being utilized, because the low temperatures pose nontrivial technical difficulties in conversion to useful work.[12,13] Therefore, developing technologies that can be driven by low-grade heat will lower the environmental footprint of desalination and enhance overall sustainability.[15−17]

Donnan dialysis (DD) is an ion-exchange membrane (IEM) process that employs the membrane as a charge-selective

Received: May 1, 2022
Revised: June 16, 2022
Accepted: June 16, 2022
Published: June 27, 2022

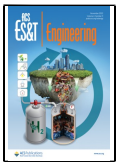

https://doi.org/10.1021/acsestengg.2c00152
ACS EST Engg. 2022, 2, 2076−2085

barrier and utilizes electrochemical potential gradients generated by two different electrolyte solutions to drive spontaneous exchange of ions.[18,19] (The acronym DD in this study refers to Donnan dialysis instead of diffusion dialysis, a related IEM process.) Unlike electricity-powered RO and ED (for hydraulic pressures and electric currents, respectively), DD is driven by the intrinsic chemical potential energy of the two solutions and, thus, does not require an external driving force. DD has been investigated for various water and environmental applications, such as groundwater treatment,[20−22] nutrient recovery,[23,24] and metal ion removal and enrichment.[25] In a past effort to deploy DD for desalination, strong acids and bases utilized the high concentrations of protons and hydroxides to demineralize saline feeds.[26,27] However, the technique, termed neutralization dialysis, requires continuous replenishments of large amounts of acids and bases and is, hence, not a practical desalination strategy.[28]

In this study, we present an innovative DD desalination approach utilizing a thermally recoverable solute of ammonium bicarbonate, NH_4HCO_3. Application of the Donnan equilibrium principles to the process is first introduced. The technology is validated by proof-of-concept experiments simulating the desalination of brackish feed streams. DD at different feed and receiver solution concentrations was then investigated, and inefficiencies intrinsic to the process were analyzed. Module-scale operation strategies were assessed using the experimental findings to elucidate the desalination performance achievable in practical applications. Lastly, broader implications of the study are discussed.

WORKING PRINCIPLES

Principles of DD. A detailed description of DD can be found in the literature and is briefly presented here.[18,19] The schematic of Figure 1A illustrates the working principles of DD across a cation exchange membrane (CEM) with fixed negative charges. The feed and receiver electrolytes are AX_a and BX_b, respectively, where A^{a+} and B^{b+} are counterions and X^- represents a single species of co-ion or a mixture of anions. An IEM of ideal permselectivity allows transport of counterions, A^{a+} and B^{b+}, in both directions but excludes co-ion X^- permeation. The concentration gradients of A^{a+} and B^{b+} between the feed and receiver chambers drive the redistribution of counterions across the membrane while maintaining electroneutrality, that is, 1 mol of A^{a+} is exchanged with a/b moles of B^{b+}, but co-ions are retained. At the equilibrium state of the dialysis process, that is, Donnan equilibrium, the electrochemical potential of each counterion is equal between the two chambers, and an electrostatic potential difference, termed the Donnan potential, is set up across the IEM. Because the same Donnan potential applies to different counterion species, distribution of A^{a+} and B^{b+} between the feed and receiver chambers is governed by the Donnan equilibrium

$$\left(\frac{c_A^F}{c_A^R}\right)^{1/a} = \left(\frac{c_B^F}{c_B^R}\right)^{1/b} \quad (1)$$

where c denotes concentration, a and b represent the ion valency, subscripts A and B indicate the counterions, and superscripts F and R signify the feed and receiver chambers, respectively. Derivation of the Donnan equilibrium, eq 1, is detailed in the Supporting Information.

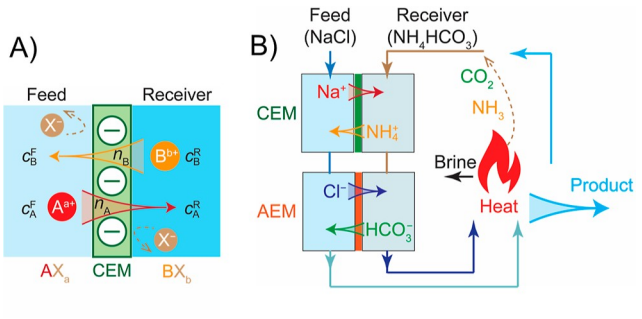

Figure 1. (A) Schematic illustrating the working principles of DD across a CEM, with feed and receiver electrolytes of AX_a and BX_b, respectively. n moles of counterions of A^{a+} and B^{b+} cations are exchanged, whereas co-ions of X^- are rejected by the charge-selective membrane. Ion concentrations are denoted by c; feed and receiver are designated by superscripts F and R, respectively; and A^{a+} and B^{b+} ions are indicated by subscripts A and B, respectively. (B) Schematic diagram of the proposed DD desalination using a thermally recoverable solute of NH_4HCO_3. The saline feed stream, with NaCl as the main solute, and the receiver stream of concentrated NH_4HCO_3 are sequentially flowed across a CEM and then an anion exchange membrane (AEM) in two DD cells. Na^+ and NH_4^+ are exchanged in the CEM cell, whereas Cl^- and HCO_3^- are swapped in the AEM cell. The large concentration gradients of NH_4^+ and HCO_3^- across the IEMs set up electrostatic potentials that are in excess of the chemical potentials of Na^+ and Cl^-, enabling the uphill transport of NaCl into the receiver stream. This leads to a large portion of NaCl in the feed being removed and replaced by NH_4HCO_3. Both streams are then heated to volatilize NH_3 and CO_2 for receiver solute recovery. Consequently, the feed stream is desalinated, while the residual receiver stream is discharged as the concentrate effluent.

For n_A moles of A^{a+} ions transported across the IEM, charge balance requires the reverse permeation of n_B moles of B^{b+}, such that

$$an_A = bn_B \quad (2)$$

Substituting eq 2 into eq 1

$$\left(\frac{c_{A,0}^F - \frac{n_A}{V^F}}{c_{A,0}^R + \frac{n_A}{V^R}}\right)^{1/a} = \left(\frac{c_{B,0}^F + \frac{n_B}{V^F}}{c_{B,0}^R - \frac{n_B}{V^R}}\right)^{1/b} \quad (3)$$

where $c_{i,0}$ is initial concentration and V is chamber volume. Solving eqs 2 and 3 simultaneously with initial conditions of the feed and receiver streams yields the moles of ion permeated, n_A and n_B, and, hence, the concentrations of A^{a+} and B^{b+} at Donnan equilibrium. By using sufficiently high concentrations of B^{b+} in the initial receiver stream, $c_{B,0}^R$, a majority of A^{a+} ions in the initial feed stream can be driven across the CEM, to achieve $c_A^R \gg c_A^F$. DD across anion exchange membranes (AEMs) follows the same principles, except that the charges are opposite. Note that no external electric voltage or current is applied in DD, unlike in ED; that is, the process is solely driven by chemical potential energy embedded in the concentration gradients between the two streams and does not require an external work input.

Desalination Using DD with Thermally Recoverable Solutes. Here, we introduce a novel desalination approach that is based on the principles of DD and utilizes thermally recoverable solutes. Working principles of the technique are illustrated by the schematic in Figure 1B. The saline feed stream and the receiver stream flow, stepwise, across a CEM

https://doi.org/10.1021/acsestengg.2c00152
ACS EST Engg. 2022, 2, 2076−2085

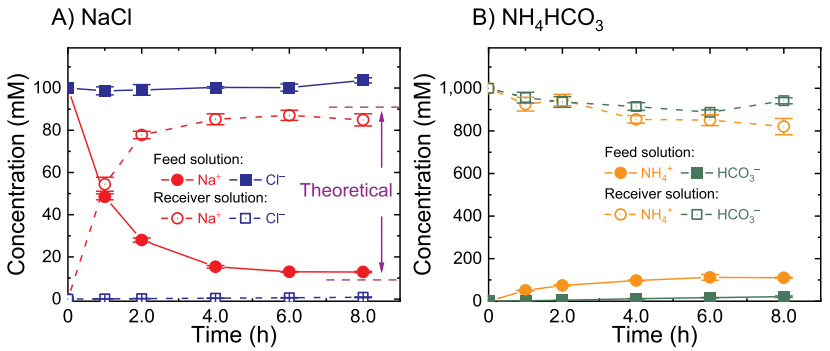

Figure 2. Ion concentrations as functions of time during CEM DD with 100 mM NaCl as feed solution and 1,000 mM NH_4HCO_3 as receiver solution: (A) Na^+ and Cl^- denoted by red circle and blue square symbols, respectively; (B) NH_4^+ and HCO_3^- denoted by yellow circle and green square symbols, respectively. Feed and receiver solution concentrations are represented by solid and open symbols, respectively. Effective area of CEM is 9.0 cm^2. Violet dashed lines indicate the theoretical equilibrium concentrations of Na^+ (9.1 mM for the feed and 90.9 mM for the receiver). Data points and error bars are mean and standard deviation, respectively, of at least duplicate experiments.

and then an AEM in two DD cells. In this illustration, the saline feed stream is a NaCl solution, whereas the receiver stream is a concentrated ammonium bicarbonate (NH_4HCO_3) solution. In the CEM cell, the concentration gradients set up a Donnan potential across the membrane to drive the transport of NH_4^+ in the receiver chamber to the feed chamber, while an equal amount of Na^+ from the feed stream permeates to the receiver chamber. The co-ions, Cl^- and HCO_3^-, are retained by the anion-excluding CEM. Correspondingly, in the AEM cell, HCO_3^- and Cl^- are exchanged, whereas Na^+ and NH_4^+ cations are rejected by the membrane, and hence, their concentrations in the feed and receiver streams remain unchanged. Overall, Na^+ and Cl^- in the feed stream are replaced with an equal amount of NH_4^+ and HCO_3^- in CEM and AEM cells, respectively (eq 2); that is, the total molar concentration of solutes in the feed stream stays the same.

Based on eq 1 with $a = b = 1$, the DD equilibria are described by $c^F_{Na+}/c^R_{Na+} = c^F_{NH_4^+}/c^R_{NH_4^+}$ and $c^F_{Cl-}/c^R_{Cl-} = c^F_{HCO_3^-}/c^R_{HCO_3^-}$ for cations and anions, respectively, and equilibrium concentrations of the four ions can be determined using eq 3. By using sufficiently high NH_4HCO_3 concentrations in the receiver stream, the resultant Donnan potential can drive the exchange of ions such that a majority of NaCl is removed from the saline feed stream and replaced by NH_4HCO_3. For example, with equal volume chambers in the two DD cells, ≈90% of the initial NaCl can be separated from the saline feed if the receiver stream is 10 times more concentrated in NH_4HCO_3.

After DD across the CEM and AEM, both the feed and receiver streams are then heated to moderate temperatures of ≈60 °C to volatilize NH_3 and CO_2 from the aqueous solutions,[29] yielding desalinated product water and concentrate streams (from the feed and receiver streams, respectively). Part of the desalinated product water, after cooling down, is diverted for the influent receiver stream of the next cycle. The volatilized ammonia and carbon dioxide are captured by the ambient temperature receiver stream, reacting to form ammonium and bicarbonate ions, that is, $NH_3 + H_2O + CO_2 \rightarrow NH_4^+ + HCO_3^-$.[30,31] The receiver solute of NH_4HCO_3 is, in principle, not consumed during the process. By substituting feed salts with the thermally recoverable NH_4HCO_3 in the DD cells and stripping the volatile solutes at moderate temperatures, the overall process utilizes low-grade heat to achieve desalination of saline feeds.

MATERIALS AND METHODS

Materials and Chemicals. The receiver solute, ammonium bicarbonate, NH_4HCO_3, was purchased from Acros Organics (Fair Lawn, NJ). Sodium chloride, NaCl, was procured from Alfa Aesar (Ward Hill, MA). All chemicals were reagent grade and were used as received. Commercial CEM Selemion CMV and AEM Selemion AMV were acquired from Asahi Glass (Tokyo, Japan).

DD Experiments. Customized single-membrane DD cells were 3D-printed and assembled. A CEM or AEM with an area of 3.0 cm × 3.0 cm separated two 3D-printed dialysis chambers of the feed and receiver solutions. 20 mL of NaCl feed solution and an equal volume of NH_4HCO_3 were introduced into the two chambers and vigorously stirred. The DD experiments were conducted as batch processes, but the conditions were also representative of continuous operation with the solutions circulated cocurrently at equal volumetric flowrates. A schematic of the experimental apparatus is shown in Figure S5 of the Supporting Information. Proof-of-concept DD experiments were carried out with 1000 mM NH_4HCO_3 as the receiver solution and 100 mM NaCl simulating brackish feed water of 5800 ppm TDS. Different feed and receiver concentrations were then used to investigate DD performance. Specifically, the feed NaCl concentration was varied between 100 and 1000 mM, with the receiver NH_4HCO_3 concentration fixed at 1000 mM. Receiver NH_4HCO_3 concentrations between 100 and 1000 mM were then examined while the feed NaCl concentration was maintained at 100 mM.

Concentration Measurements. Four ions of the electrolyte solutions, that is, Na^+, Cl^-, NH_4^+, and HCO_3^-, were characterized in the study. Na^+, NH_4^+, and Cl^- concentrations were quantified by ion chromatography, IC (Dionex Aquion, Thermo Fisher Scientific, Waltham, MA). The cations, Na^+ and NH_4^+, were characterized by cation column Dionex IonPac CS16, whereas the anion concentration of Cl^- was analyzed by IonPac AS22 from Thermo Fisher Scientific. HCO_3^- concentrations of the samples were determined by total inorganic carbon analysis using a total organic carbon analyzer (QbD1200, Hach, Loveland, CO).

RESULTS AND DISCUSSION

DD of Brackish Feed. The desalination of brackish groundwater (defined as having TDS concentration of 1000−10,000 ppm)[32] is an important alternative to address

https://doi.org/10.1021/acsestengg.2c00152
ACS EST Engg. 2022, 2, 2076−2085

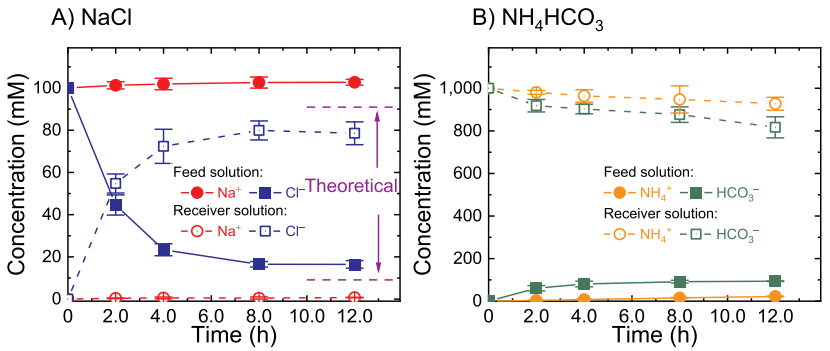

Figure 3. Ion concentrations as functions of time during AEM DD with 100 mM NaCl as feed solution and 1,000 mM NH_4HCO_3 as receiver solution: (A) Na^+ and Cl^- denoted by red circle and blue square symbols, respectively; (B) NH_4^+ and HCO_3^- denoted by yellow circle and green square symbols, respectively. Feed and receiver solution concentrations are represented by solid and open symbols, respectively. Effective area of AEM is 9.0 cm^2. Violet dashed lines indicate the theoretical equilibrium concentrations of Cl^- (9.1 mM for the feed and 90.9 mM for the receiver). Data points and error bars are mean and standard deviation, respectively, of at least duplicate experiments.

freshwater shortages, especially in inland areas.[5,33,34] To demonstrate proof-of-concept, DD of a simulated brackish water feed of 100 mM NaCl (5800 ppm TDS) was investigated. The batch experiments utilized either CEM or AEM in the dialysis cell and 1000 mM NH_4HCO_3 in the receiver chamber. Equal volumes were used for the feed and receiver solutions. The feed and receiver solutions were periodically sampled and analyzed for Na^+, Cl^-, NH_4^+, and HCO_3^- concentrations to study mass transfer of the dialysis processes.

Figure 2 presents results of the CEM DD experiments, where the concentration difference of NH_4^+ drives the exchange with Na^+. Na^+ concentration in the feed chamber drops from 100 mM initially to 12.8 ± 0.3 mM at 8.0 h (Figure 2A). Correspondingly, $[Na^+]$ in the receiver chamber rises to 84.9 ± 2.9 mM. Importantly, even after $[Na^+]$ of the receiver stream exceeds that of the feed stream (at ≈1.0 h), Na^+ ions continue to be transported against the concentration gradient; that is, uphill transport is achieved. Na^+ concentrations in the feed and receiver solutions are close to the Donnan equilibrium values of 9.1 and 90.9 mM, respectively (indicated by dashed violet lines), as determined by eq 3. A decreasing mass transfer rate of Na^+ is observed as DD progresses: 59% of the change in Na^+ concentration occurred in the first hour and only 3% from 4.0 to 8.0 h. This trend is consistent with the expected gradual diminishing of the driving force for Na^+ transport in batch experiments as the solution concentrations approach Donnan equilibrium.[35−38] Meanwhile, the negatively charged CEM effectively blocks Cl^- permeation from the feed chamber to the receiver chamber. At the end of the experimental run (8.0 h), only 0.867 ± 0.178 mM of Cl^- accumulated in the receiver chamber, with >99% of Cl^- retained in the feed chamber. It is important to note that, although Cl^- permeation in the CEM DD and Na^+ permeation in the AEM DD are unintended co-ion transports, the co-ion leakage is not actually detrimental to the desalination performance of the overall process, as the ultimate aim is to remove Na^+ and Cl^- from the feed and into the receiver.

The transport of Na^+ is driven by NH_4^+ permeation in the opposite direction. After 8.0 h, NH_4^+ in the feed chamber reaches 110 ± 2 mM (Figure 2B). The change in feed stream $[NH_4^+]$ does not match up with the increase in receiver stream $[Na^+]$ of 84.9 ± 2.9 mM. This is because the CEM is not perfectly selective for cation transport and some anions of HCO_3^- undesirably leak into the feed chamber due to the concentration gradient across the membrane. Final $[HCO_3^-]$ in the feed stream is 21.3 ± 3.4 mM, and HCO_3^- permeation is within 20% of NH_4^+ transport. Co-ion leakage is further analyzed and discussed later. Additionally, NH_4HCO_3 concentrations in the receiver chamber dropped by ≈4% at the end of the experiments. This decrease is attributed to two effects: osmotic water transport and volatility of $NH_{3(aq)}$ and $CO_{2(aq)}/H_2CO_{3(aq)}$. As the receiver solutions are more concentrated than the feed solutions, the osmotic pressure difference drives water flux from the feed to the receiver, diluting the receiver solution. Osmotic water transport is further discussed in the Supporting Information. Additionally, some $NH_{3(g)}$ and $CO_{2(g)}$ volatilized from the solutions, likely due to vigorous stirring and during sampling. Although the apparatus and experimental protocol were designed to minimize exposure of the solutions to the atmosphere (e.g., the reactor was capped), the system was not hermetically sealed.

The trends of ion concentrations in AEM DD (Figure 3) resemble the CEM experiments, except that the counterions exchanged are Cl^- and HCO_3^- anions. Cl^- concentration in the feed chamber decreases from 100 to 16.4 ± 1.8 mM, while the receiver concentration rises to 78.5 ± 5.4 mM. The equilibrium feed concentration of Cl^- (16.4 mM) is 7.3 mM higher than the theoretical calculation (9.1 mM) denoted by the violet dashed line. The deviation of 7.3 mM is larger than the 3.7 mM difference in the CEM test and can be attributed to the lower permselectivity of the commercial AEM, Selemion AMV, compared to the CEM, Selemion CMV. This issue will be further discussed in the next section. Similar to the uphill mass transfer of Na^+ in CEM DD, $[Cl^-]$ in the feed surpasses the receiver after ≈2.0 h in the AEM experiments and continues to transport against the concentration gradient. As the electrochemical potential driving ion transport is depleted, a decreasing mass transfer rate is observed: 66% of the change in Cl^- concentration is achieved in the initial 2 h and only 8% from 4.0 to 8.0 h. The kinetics of anion exchange is overall slower than that of CEM DD because the Selemion AMV has lower ion conductance compared to the CEM.[39,40] Meanwhile, co-ion Na^+ leaks across the AEM to the receiver chamber and accumulates to 0.731 ± 0.112 mM, which is negligible compared to $[Cl^-]$. The HCO_3^- exchanged to the feed chamber is 93.8 ± 1.3 mM, and 22.4 ± 1.3 mM NH_4^+ permeates across the AEM to the feed chamber (Figure 3B). Similarly, water osmosis and volatilization lower NH_4HCO_3

https://doi.org/10.1021/acsestengg.2c00152
ACS EST Engg. 2022, 2, 2076−2085

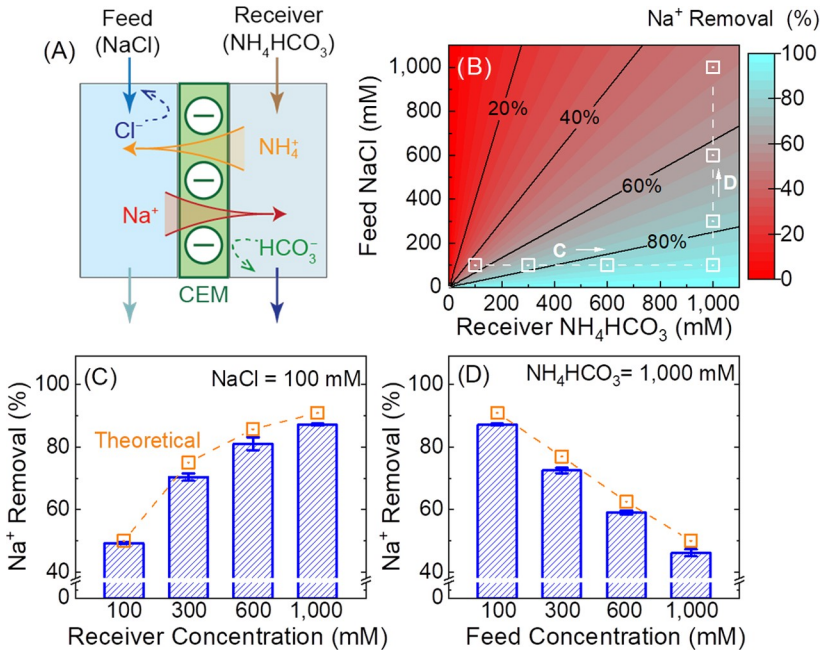

Figure 4. (A) Schematic of CEM DD, with ion exchange indicated. (B) Heat map of theoretical Na^+ removal with different combinations of feed and receiver concentrations, with blue and red regions denoting high and low removals, respectively. White square symbols with connecting dashed lines correspond to theoretical removals for the experimental conditions in (C,D). Experimental Na^+ removal (blue columns) of DD across CEM is shown as a function of (C) receiver solution concentration, with feed salinity of 100 mM NaCl, and (D) feed salinity, with receiver solution of 1000 mM NH_4HCO_3. Experimental Na^+ removals are reported at either 8.0 h (all four conditions of C and 100 mM of D) or 12.0 h (300, 600, and 1000 mM of D) of the DD test runs. Orange square symbols represent the predicted Na^+ removal based on Donnan equilibrium (eqs 2 and 3), i.e., white square symbols in (B). Data points and error bars are mean and standard deviation, respectively, of at least duplicate experiments.

concentration in the receiver solution by ≈50−80 mM NH_4HCO_3 during the 12 h experiments, partially contributing to the discrepancy between the experimental equilibrium of Cl^- and the theoretical values (blue square symbols and dashed violet lines in Figure 3A, respectively).

The CEM and AEM dialysis experiments on brackish salinity validate the concepts of DD desalination. The uphill transport of counterions in DD was effective in lowering the feed NaCl content beyond the equal concentration point (both feed and receiver streams at 50 mM). Feed $[Na^+]$ and $[Cl^-]$ at the end of the batch operations was in the freshwater range (<1000 ppm TDS or equivalently 17 mM NaCl),[41,42] which is also the level of acceptable palatability by the World Health Organization.[43] In the following sections, we (i) investigate the influence of key operating parameters, specifically, feed salinity and receiver concentration, on DD desalination performance; (ii) examine the inefficiencies arising from imperfect co-ion rejection; and (iii) explore alternative flow configurations, in particular, countercurrent operation, to improve performance.[44,45] Additionally, although the desalination strategy presented in Figure 1 shows two DD exchange cells connected in series, it is not necessary to flow the streams stepwise through two cells separately for cation and anion exchange. The simultaneous operation of CEM and AEM DD in a combined cell would yield comparable NaCl removal, as demonstrated in Figure S13 of the Supporting Information.

Principles of DD Govern Salt Removal. The performance of DD desalination at different feed and receiver concentrations was further investigated. CEM DD was employed for the investigation (Figure 4A), with the volume ratio of feed to receiver solution maintained at 1:1. Figure 4B presents the theoretical Na^+ cation removals, based on Donnan equilibrium (eq 3), across a range of feed and receiver concentrations. The heat map shows the percentage of Na^+ concentration drop relative to the initial feed concentration (red and blue regions denote low and high Na^+ removal, respectively), with the contour lines demarcating 20, 40, 60, and 80% removal. As expected, the theoretical analysis indicates that a higher receiver NH_4HCO_3 concentration will extract more target Na^+ (and, equivalently, Cl^-) from the feed stream. For instance, for a feed concentration of 100 mM NaCl, the removal rises from 50.0 to 90.9% when the receiver concentration is elevated from 100 to 1000 mM NH_4HCO_3. Notably, a 600 mM NH_4HCO_3 receiver solution can already exchange and extract 85.7% of the Na^+ ions from the feed; that is, removal is only ≈5% lower, while the receiver concentration is 40% less compared to utilizing 1,000 mM NH_4HCO_3. This is reflected in the relatively gentle slopes of the high removal (e.g., 80%) contour lines in Figure 4B. Therefore, it is an option to utilize a much less concentrated receiver solution for a slightly reduced but still acceptable desalination performance. The analysis also indicates that using the same receiver solution to treat feed streams with higher salinities leads to lower salt removal. For example, the removal drops from 90.9 to 50.0% when the feed NaCl concentration increases from 100 to 1000 mM, with a receiver concentration of 1,000 mM NaCl.

CEM DD experiments of different feed and receiver concentrations were performed to verify the theoretical assessments. Experimental ion concentrations as functions of time can be found in the Supporting Information. Figure 4C shows the Na^+ removed from an initial 100 mM NaCl feed stream using different receiver concentrations. The experimental removals are 49.3 ± 0.3, 70.4 ± 1.2, 81.0 ± 2.0, and 87.2 ± 0.3% for 100, 300, 600, and 1000 mM NH_4HCO_3 receiver solutions, respectively (columns). Compared to the

https://doi.org/10.1021/acsestengg.2c00152
ACS EST Engg. 2022, 2, 2076−2085

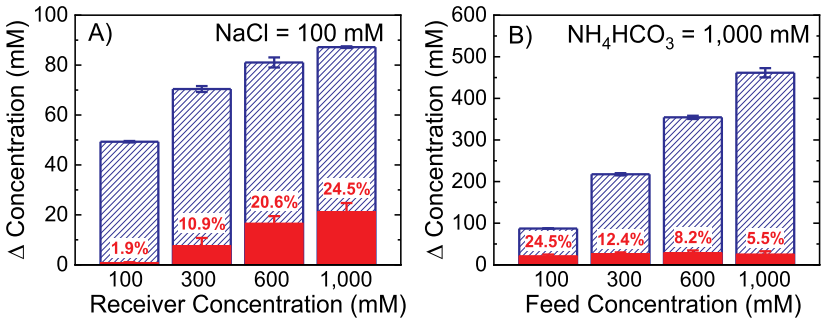

Figure 5. Concentration changes of Na^+ target counterion and HCO_3^- co-ion, blue and red columns, respectively, for DD across CEM as a function of: (A) receiver solution concentration, with feed salinity of 100 mM NaCl, and (B) feed salinity, with receiver solution of 1000 mM NH_4HCO_3. The labels indicate the percentage of undesirable HCO_3^- leakage relative to experimentally measured Na^+ removal. Concentration changes are measured after 8.0 h (A and 100 mM of B) or 12.0 h (300, 600, and 1000 mM of B) of dialysis across effective CEM area of 9.0 cm^2. Data points and error bars are mean and standard deviation, respectively, of at least duplicate experiments.

theoretical calculations of 50.0, 75.0, 85.7, and 90.9% (square symbols), the experimental results are only marginally lower (≈1−5%). Similarly, small deviations between theoretical and experimental Na^+ removals are obtained when the feed salinity is varied (Figure 4D). The percentage of Na^+ removal drops from 87.2 ± 0.3 to 72.5 ± 0.9%, 59.1 ± 0.6, and 46.2 ± 1.1% when the feed salinity of NaCl increases from 100 mM to 300, 600, and 1000 mM, respectively, with the same initial receiver concentration of 1000 mM NH_4HCO_3. The discrepancies between the experimental measurements and theoretical predictions (90.9, 76.9, 62.5, and 50.0%) are, again, within 5%. The good agreement between experiments and theory across a wide range of feed and receiver concentrations (0−1000 mM) establishes that the principles of Donnan equilibrium hold up in quantitatively determining the ion exchange in DD, thus providing the basis for analysis of operating strategy design for DD desalination (presented later). Additionally, it is worthwhile to note that feed concentrations of 600−1000 mM NaCl exceed the typical salinity of seawater (≈600 mM or 35 g/L NaCl),[46,47] indicating the potential to desalinate streams beyond brackish salinities.

The small deviations (<5%) of the experimental results from the ideal Donnan equilibria are caused by three effects. The imperfect permselectivity of IEMs is the primary cause of the marginally incomplete ion exchange. As the membranes are not completely selective for counterions, receiver solution co-ions (HCO_3^- for Figure 4) leak into the feed stream. To maintain net electroneutrality, receiver co-ion leakage is counterbalanced by permeation of an equivalent charge of receiver counterions in the same direction (NH_4^+ to feed) and feed co-ions in the opposite direction (Cl^- to receiver). While the latter would not negatively affect the overall goal of removing NaCl from the saline feed stream, the former phenomenon of receiver counterion co-transport would reduce the Donnan potential to drive exchange with feed counterions (Na^+ for the results presented in Figure 4). Therefore, receiver co-ion leakage due to imperfect membrane permselectivity eventually causes less Na^+ removal. The detrimental effects of co-ion leakage are further analyzed in the next section. The second reason is the lowered receiver NH_4HCO_3 concentrations due to water osmosis and volatilization loss. Magnitude of the osmotic water fluxes becomes significant with large feed-receiver concentration differences. Also, volatilization of $NH_{3(g)}$ and $CO_{2(g)}$ is more pronounced in highly concentrated receiver solutions. The slightly diminished NH_4^+ receiver concentrations due to water osmosis and volatilization lower the DD driving forces and, consequently, Na^+ removal. Actual DD desalination processes should, in principle, be able to operationally mitigate the two losses by careful design, such as confining the stream volumes and hermetically sealing the setup. Lastly, eq 3 used to calculate the concentrations at Donnan equilibrium did not factor in activity coefficients of the species and weak acid/base speciations of ammonium and bicarbonate. These simplifications expectedly contribute to some of the deviations between experimental results and theoretical values. A more accurate assessment can be obtained by employing eq S5 in the Supporting Information, where the activity coefficients of individual ions in a complex mixture are included and the protonation−deprotonation of ammonium and bicarbonate is incorporated. Nonetheless, the good agreement of the experimental results with theoretical projections shows that eq 3 is sufficient for quantitative estimation of DD end points.

Detrimental Effects of Co-Ion Leakage Are Marginal. The main inefficiency of DD desalination is the co-ion leakage across the charged membranes. However, as discussed earlier, leakage of salt co-ions from the feed to the receiver stream, that is, Cl^- in CEM DD and Na^+ in AEM DD, is not actually deleterious to the overall goal of removing NaCl from the saline feed stream. Crucially, the leakage of salt co-ions does not negatively impact the counterion concentrations at Donnan equilibrium. Rather, it is the co-ion leakage of receiver solutes, that is, HCO_3^- in CEM DD and NH_4^+ in AEM DD, that diminishes the Donnan potential driving force for removal of salt counterions from the feed solution and constrains the process from reaching the full theoretical thermodynamic limit for desalination. Using CEM DD to illustrate this point, some NH_4^+ permeating from the receiver to feed would be to offset the flux of charges carried by the leakage of co-ion HCO_3^- in the same direction (Cl^- transport in the opposite direction also contributes to balancing the charge), thus reducing the total Na^+ that exchanges from the feed into the receiver solution. This detrimental effect is quantitatively expressed in eq S4: the leakage of receiver co-ions raises the feed concentration and consequently reduces the Donnan potential; therefore, Na^+ extracted from feed to receiver is lessened. Subsequently, when the CEM-treated stream flows on next to the anion DD cell, the presence of HCO_3^- in the feed would lower the Donnan potential for Cl^- removal and result in a higher equilibrium feed concentration for Cl^-. Both Donnan potential reductions

https://doi.org/10.1021/acsestengg.2c00152
ACS EST Engg. 2022, 2, 2076−2085

in CEM and AEM DD undermine the desalination efficiency of the overall process.

Figure 5 compares the unintended co-ion leakage of HCO_3^- with desired Na^+ removal in CEM DD (filled red and patterned blue columns denote the concentration change in the feed and receiver solutions, respectively) using different feed and receiver concentrations. The detailed profiles of ion concentrations as functions of time in each experiment are presented by Figures S7−S12 in the Supporting Information. When the feed is 100 mM NaCl and the receiver NH_4HCO_3 concentrations are 100, 300, 600, and 1,000 mM (Figure 5A), the HCO_3^- concentrations in the feed chamber at the end of the experiments (8.0 h) are 0.94 ± 0.04, 7.7 ± 3.0, 16.7 ± 2.8, and 21.3 ± 3.4 mM, respectively. The HCO_3^- co-ions that leaked across the CEM and accumulated in the feed stream are equivalently 1.9, 10.9, 20.6, and 24.5% of the Na^+ reduction (indicated by labels above the filled red columns). Raising the receiver concentration from 100 to 1000 mM increases the average fluxes of HCO_3^- permeation from 2.6 to 59.3 × 10^{-3} mol m^{-2} h^{-1}, due to the larger driving force for ion exchange.

Figure 5B shows the change in concentrations of Na^+ and HCO_3^- in the receiver and feed solutions, respectively, for different feed salinities, while the receiver is 1000 mM NH_4HCO_3. Except for the 100 mM NaCl feed solution experiment, which was sampled at 8.0 h, all concentrations were characterized after 12.0 h. Final HCO_3^- in the feeds when desalinating 100, 300, 600, and 1000 mM NaCl are 21.3 ± 3.4, 27.0 ± 2.8, 28.9 ± 5.5, and 25.6 ± 6.9 mM, respectively, corresponding to 24.5, 12.4, 8.2, and 5.5% of the Na^+ feed concentration drop. The average fluxes of HCO_3^- permeation are similar for the different feed NaCl concentrations (47.4−59.3 × 10^{-3} mol m^{-2} h^{-1}). Comparison of final feed HCO_3^- concentrations between Figure 5A and B provides evidence that the co-ion leakage of HCO_3^- in CEM DD and NH_4^+ in AEM DD is primarily determined by the initial NH_4HCO_3 concentration in the receiver stream; feed salinity plays a relatively minor role. Therefore, to suppress unfavorable solute leakage, it will be beneficial to utilize a low receiver concentration while still obtaining operationally adequate NaCl removal from the feed stream, as informed by the trends of Figure 4.

Crucially, even the highest percentage of HCO_3^- leakage compared to Na^+ reduction reported here (24.5%) only marginally affects the demineralization performance. Specifically, the percentage of 24.5%, corresponding to the accumulation of 21.3 mM of HCO_3^- in the feed chamber in DD with 100 mM NaCl-1000 mM NH_4HCO_3 theoretically leads to only ≈2% reduction in Na^+ removal. This is corroborated by the experimental results presented in Figure 4, where the deviation from ideal Na^+ removal is <4% for the same feed and receiver concentrations (other inefficiencies, discussed earlier, contribute to the actual difference). Therefore, using IEMs with higher permselectivities, that is, better rejection of co-ions, can improve performance in DD desalination, but the enhancements will likely not be dramatic, that is, current IEMs are sufficiently selective. In addition, the durations of the experiments presented in Figure 5 were deliberately protracted to ensure that the end states are close to equilibrium. However, as the process approaches Donnan equilibrium, Na^+ permeation gradually vanishes (electrochemical driving force is depleted) while HCO_3^- continues to leak across the membrane due to the sustained concentration gradient. This difference between counterion and co-ion fluxes can be observed in the rates of concentration changes in Figures 2 and 3. In other words, Figure 5 overestimates the co-ion leakage actually necessary to exploit the Donnan potentials for desalination and presents overly conservative assessments on the efficiencies. In practical applications, dialysis times can be shortened without appreciably compromising Na^+ and Cl^- removals, thus greatly lessening the unfavorable accumulations of HCO_3^- and NH_4^+ in the feed streams (Figures S7−S12 in the Supporting Information). Overall, co-ion leakage, although unavoidable, does not significantly affect DD desalination.

Countercurrent Operation Achieves Greater Salt Removal and Recovery Yield Performance. The proof-of-concept demonstration of DD desalination and the analysis of the influences of feed and receiver solution concentrations are essentially batch experiments. In actual operations, the design space of a continuous process will be significantly broader, including various flow configurations and different ratios of feed/receiver volumetric flow rates. In particular, countercurrent operation, where the two streams flow in opposite directions across the membrane, is able to achieve higher separation performance.[44,45,48] NaCl removals and water recovery yields were analytically evaluated for cocurrent and countercurrent flow configurations. In the study thus far, the initial feed streams were pure NaCl solutions, whereas the starting receiver streams contained only NH_4HCO_3. However, for DD desalination where a portion of the desalinated product water is recirculated back to redissolve the volatilized $NH_{3(g)}$ and $CO_{2(g)}$ and serve as the entering receiver stream (Figure 1B), there will be some NaCl in the initial receiver solution. Also, as discussed earlier, receiver co-ions of HCO_3^- and NH_4^+ can leak across the CEM and AEM, respectively, and accumulate in the feed stream, negatively affecting ion exchange in the next DD cell. These effects are incorporated into the analysis to better estimate the performance of practical DD desalination. Specifically, 30 mM NH_4HCO_3 is included in the 100 mM NaCl feed streams to simulate the co-ion leakage, and the receiver streams of 1000 mM NH_4HCO_3 have 23 mM NaCl to simulate residual salt in the partially diverted product water (note that the salt concentration is higher than typical salinities of potential product streams). Additionally, different volumetric ratios of feed to receiver streams were considered. The methodology is further detailed in the Supporting Information, and the results are presented in Figure 6.

Cocurrent DD with a feed/receiver volumetric ratio of 2:1 delivered a 22.6 mM NaCl product stream (77.4% removal, patterned blue column, left vertical axis of Figure 6) with 50.0% recovery yield (filled green column, right vertical axis) for the overall desalination. In general, even lower product water salinities can be attained but at the cost of smaller recovery yields (Figures S4 of the Supporting Information). In sharp contrast, markedly improved performance is achieved in countercurrent mode: 95.5% of NaCl can be removed even with 87.5% recovery yield (8:1 feed/receiver volumetric ratio). Importantly, the exiting concentrate contains 787 mM NaCl, 7.9-fold greater than the initial feed salinity. In other words, both the product water salinity and brine volume can be significantly reduced in countercurrent operation, with most of the salt concentrated in the exiting brine (additional results can be found in the Supporting Information, Figures S4). Crucially, countercurrent mode allows the use of less concentrated receiver solutions while still meeting adequate desalination performance; for example, replacing 1000 mM with 600 mM

https://doi.org/10.1021/acsestengg.2c00152
ACS EST Engg. 2022, 2, 2076−2085

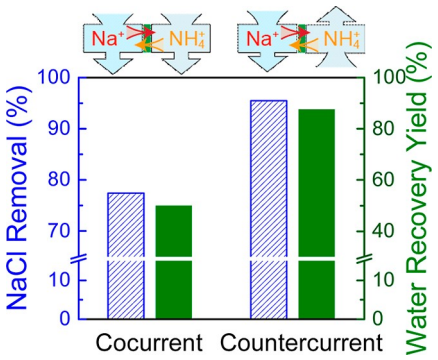

Figure 6. Projected salt removal (blue shaded columns, left vertical axis) and water recovery yield (green solid columns) for cocurrent and countercurrent DD operation of brackish water desalination, with feed of 100 mM NaCl with 30 mM NH_4HCO_3 and receiver of 1000 mM NH_4HCO_3 with 23 mM NaCl.

NH_4HCO_3 can obtain 87.7% Na^+ removal at 80.0% recovery yield. Utilizing lower receiver solution concentrations can mitigate co-ion leakage and solute loss due to volatilization. Therefore, the potential of DD desalination can be better exploited in a scheme described by Figure S3B. The influent feed passes through the DD cells, while the receiver solution flows in countercurrent direction and exchanges the salts out from the feed. Low-grade heat then volatilizes ammonia and carbon dioxide from both streams to yield concentrated brine and product water. A small portion of the product water would be diverted to redissolve the gases and form ammonium bicarbonate, thus reconstituting the receiver solution.

IMPLICATIONS

In this study, we presented a novel process that combines DD and a thermally recoverable solute, NH_4HCO_3, to enable the utilization of low-grade heat for desalination. Saline feeds of 100 mM NaCl were desalinated to <17 mM NaCl (1000 ppm TDS) as proof-of-concept demonstration. The investigation further showed that ion transfers across the IEMs are governed by the classic principles of Donnan equilibrium. The main inefficiency was identified to be the co-ion leakage of receiver solutes, that is, HCO_3^- in CEM dialysis and NH_4^+ in AEM dialysis, which limits DD from fully realizing the thermodynamic potential of the system. However, current commercially available IEMs are sufficiently permselective to adequately suppress the co-ion leakage and yield effective desalination performance. Analysis additionally revealed that countercurrent operation can achieve substantially improved salt removals and water recovery yields compared to cocurrent flow configuration.

Improving the membrane permselectivity can further lessen the deleterious effects of co-ion leakage, whereas enhancements in membrane ionic conductivity increase the process kinetics and, consequently, lower the membrane area requirement. We point out that the commercial membranes used in this study are not optimized for the DD desalination described here. Balancing the membrane conductance with permselectivity within the bounds of the tradeoff can potentially attain better overall cost-effectiveness of desalination.[49] Membrane kinetics is a significant limiting factor for DD applications.[18] Development of IEMs with higher ionic conductivities and advances in module innovation will likely be needed to enable the actual implementation of DD technologies. Practical applications of the technology can take advantage of the ammonium receiver solute being an important nitrogen fertilizer. Using the desalinated stream for agricultural purposes, such as fertigation or hydroponic farming,[50−52] instead of end uses requiring high product water quality would relax the requirement to strip out the ammoniacal nitrogen. Targeting such fit-for-purpose applications, rather than potable water production, can considerably simplify overall operations and yield more favorable process economics. Additionally, in this proof-of-concept study, NaCl solutions were employed as the feeds. In practice, multivalent cations, for example, Ca^{2+} and Mg^{2+}, in actual saline streams can potentially form carbonate precipitates in the solutions. Potential impacts and mitigation strategies of such mineral formation would need to be further investigated.

This study focused on NH_4HCO_3 for the proof-of-concept demonstration, but other recoverable solutes can be suitable for the concept, for example, switchable polarity solvents and upper critical solution temperature salts.[53,54] We clarify that DD desalination with thermally recoverable solutes is not intended to directly compete with state-of-the-art RO in the large-scale potable water supply. Rather, it can be an alternative for niche applications, such as the example of agricultural water production. In particular, instead of using electricity, the innovation can utilize low-grade heat, a sizeable energy source that is currently underutilized,[11−13] to drive desalination. Lastly, further analyses are necessary to quantify the actual energy demands of the process, project the capital costs and operating expenses of facility-scale operation, and evaluate the carbon intensity of the technology.

ASSOCIATED CONTENT

Supporting Information

The Supporting Information is available free of charge at https://pubs.acs.org/doi/10.1021/acsestengg.2c00152.

Derivation of the Donnan equilibrium and analytical models for module performance, salt removal and recovery yield for different flow configurations, experimental apparatus, general properties of the IEMs, discussions on IEM water transport, experimental ion concentrations as functions of time in CEM DD, and three-chamber DD experiment (PDF)

AUTHOR INFORMATION

Corresponding Author

Ngai Yin Yip − *Department of Earth and Environmental Engineering, Columbia University, New York, New York 10027-6623, United States; Columbia Water Center, Columbia University, New York, New York 10027-6623, United States;* orcid.org/0000-0002-1986-4189; Phone: +1 212 8542984; Email: n.y.yip@columbia.edu

Author

Hanqing Fan − *Department of Earth and Environmental Engineering, Columbia University, New York, New York 10027-6623, United States*

Complete contact information is available at: https://pubs.acs.org/10.1021/acsestengg.2c00152

Notes

The authors declare no competing financial interest.

https://doi.org/10.1021/acsestengg.2c00152
ACS EST Engg. 2022, 2, 2076−2085

■ ACKNOWLEDGMENTS

We thank Dr. Brian Mailloux for his assistance in developing the ion chromatography protocols and gratefully acknowledge the editorial assistance of Peter Cruz-Grace and Devon Elizabeth Campbell.

■ REFERENCES

(1) Mekonnen, M. M.; Hoekstra, A. Y. Four Billion People Facing Severe Water Scarcity. *Sci. Adv.* **2016**, *2*, No. e1500323.
(2) Greve, P.; Kahil, T.; Mochizuki, J.; Schinko, T.; Satoh, Y.; Burek, P.; Fischer, G.; Tramberend, S.; Burtscher, R.; Langan, S.; Wada, Y. Global Assessment of Water Challenges under Uncertainty in Water Scarcity Projections. *Nat. Sustain.* **2018**, *1*, 486−494.
(3) Schewe, J.; Heinke, J.; Gerten, D.; Haddeland, I.; Arnell, N. W.; Clark, D. B.; Dankers, R.; Eisner, S.; Fekete, B. M.; Colón-González, F. J.; Gosling, S. N.; Kim, H.; Liu, X.; Masaki, Y.; Portmann, F. T.; Satoh, Y.; Stacke, T.; Tang, Q.; Wada, Y.; Wisser, D.; Albrecht, T.; Frieler, K.; Piontek, F.; Warszawski, L.; Kabat, P. Multimodel Assessment of Water Scarcity under Climate Change. *PNAS* **2014**, *111*, 3245−3250.
(4) Elimelech, M.; Phillip, W. A. The Future of Seawater Desalination: Energy, Technology, and the Environment. *Science* **2011**, *333*, 712−717.
(5) Shannon, M. A.; Bohn, P. W.; Elimelech, M.; Georgiadis, J. G.; Mariñas, B. J.; Mayes, A. M. Science and Technology for Water Purification in the Coming Decades. *Nature* **2008**, *452*, 301−310.
(6) Jones, E.; Qadir, M.; van Vliet, M. T. H.; Smakhtin, V.; Kang, S.-m. The State of Desalination and Brine Production: A Global Outlook. *Sci. Total Environ.* **2019**, *657*, 1343−1356.
(7) Fane, A. G. A Grand Challenge for Membrane Desalination: More Water, Less Carbon. *Desalination* **2018**, *426*, 155−163.
(8) Elsaid, K.; Sayed, E. T.; Abdelkareem, M. A.; Baroutaji, A.; Olabi, A. G. Environmental Impact of Desalination Processes: Mitigation and Control Strategies. *Sci. Total Environ.* **2020**, *740*, 140125.
(9) Lienhard, J. H.; Thiel, G. P.; Warsinger, D. M.; Banchik, L. D. *Low Carbon Desalination: Status and Research, Development, and Demonstration Needs, Report of a Workshop Conducted at the Massachusetts Institute of Technology in Association with the Global Clean Water Desalination Alliance*; Massachusetts Institute of Technology: Cambridge, MA, 2016.
(10) Liu, J.; Chen, S.; Wang, H.; Chen, X. Calculation of Carbon Footprints for Water Diversion and Desalination Projects. *Energy Procedia* **2015**, *75*, 2483−2494.
(11) Forman, C.; Muritala, I. K.; Pardemann, R.; Meyer, B. Estimating the Global Waste Heat Potential. *Renewable Sustainable Energy Rev.* **2016**, *57*, 1568−1579.
(12) Johnson, I.; Choate, W. T.; Davidson, A. *Waste Heat Recovery. Technology and Opportunities in US Industry*; BCS, Inc.: Laurel, MD (United States), 2008.
(13) Rahimi, M.; Straub, A. P.; Zhu, X.; Elimelech, M.; Gorski, C. A.; Logan, B. E. Emerging Electrochemical and Membrane-Based Systems to Convert Low-Grade Heat to Electricity. *Energy Environ. Sci.* **2018**, *11*, 276−285.
(14) Tester, J. W.; Anderson, B. J.; Batchelor, A.; Blackwell, D.; DiPippo, R.; Drake, E.; Garnish, J.; Livesay, B.; Moore, M.; Nichols, K. *The Future of Geothermal Energy*; Massachusetts Institute of Technology, 2006; p 358.
(15) Mathioulakis, E.; Belessiotis, V.; Delyannis, E. Desalination by Using Alternative Energy: Review and State-of-the-Art. *Desalination* **2007**, *203*, 346−365.
(16) Sansom, R. Decarbonising Low Grade Heat for Low Carbon Future. Ph.D. Thesis, Imperial College London (United Kingdom), Ann Arbor, 2014.
(17) Li, Y.; Chen, X.; Xu, Y.; Zhuo, Y.; Lu, G. Sustainable Thermal-Based Desalination with Low-Cost Energy Resources and Low-Carbon Footprints. *Desalination* **2021**, *520*, 115371.
(18) Strathmann, H. *Ion-Exchange Membrane Separation Processes*; Elsevier, 2004.
(19) Sata, T. *Ion Exchange Membranes: Preparation, Characterization, Modification and Application*; Royal Society of Chemistry, 2007.
(20) Breytus, A.; Hasson, D.; Semiat, R.; Shemer, H. Removal of Nitrate from Groundwater by Donnan Dialysis. *J. Water Process. Eng.* **2020**, *34*, 101157.
(21) Garmes, H.; Persin, F.; Sandeaux, J.; Pourcelly, G.; Mountadar, M. Defluoridation of Groundwater by a Hybrid Process Combining Adsorption and Donnan Dialysis. *Desalination* **2002**, *145*, 287−291.
(22) Sarkar, S.; SenGupta, A. K.; Prakash, P. The Donnan Membrane Principle: Opportunities for Sustainable Engineered Processes and Materials. *Environ. Sci. Technol.* **2010**, *44*, 1161−1166.
(23) Chen, C.; Dong, T.; Han, M.; Yao, J.; Han, L. Ammonium Recovery from Wastewater by Donnan Dialysis: A Feasibility Study. *J. Cleaner Prod.* **2020**, *265*, 121838.
(24) Shashvatt, U.; Amurrio, F.; Portner, C.; Blaney, L. Phosphorus Recovery by Donnan Dialysis: Membrane Selectivity, Diffusion Coefficients, and Speciation Effects. *Chem. Eng. J.* **2021**, *419*, 129626.
(25) Asante-Sackey, D.; Rathilal, S.; Kweinor Tetteh, E.; Ezugbe, E. O.; Pillay, L. V. Donnan Membrane Process for the Selective Recovery and Removal of Target Metal Ions—A Mini Review. *Membranes* **2021**, *11*, 358.
(26) Igawa, M.; Echizenya, K.; Hayashita, T.; Seno, M. Donnan Dialysis Desalination. *Chem. Lett.* **1986**, *15*, 237−238.
(27) Igawa, M.; Echizenya, K.; Hayashita, T.; Seno, M. Neutralization Dialysis for Deionization. *Bull. Chem. Soc. Jpn.* **1987**, *60*, 381−383.
(28) Chérif, M.; Mkacher, I.; Dammak, L.; Ben Salah, A.; Walha, K.; Grande, D.; Nikonenko, V. Water Desalination by Neutralization Dialysis with Ion-Exchange Membranes: Flow Rate and Acid/Alkali Concentration Effects. *Desalination* **2015**, *361*, 13−24.
(29) McCutcheon, J. R.; McGinnis, R. L.; Elimelech, M. A Novel Ammonia—Carbon Dioxide Forward (Direct) Osmosis Desalination Process. *Desalination* **2005**, *174*, 1−11.
(30) McGinnis, R. L.; McCutcheon, J. R.; Elimelech, M. A Novel Ammonia−Carbon Dioxide Osmotic Heat Engine for Power Generation. *J. Membr. Sci.* **2007**, *305*, 13−19.
(31) Cusick, R. D.; Kim, Y.; Logan, B. E. Energy Capture from Thermolytic Solutions in Microbial Reverse-Electrodialysis Cells. *Science* **2012**, *335*, 1474−1477.
(32) Stanton, J. S.; Anning, D. W.; Brown, C. J.; Moore, R. B.; McGuire, V. L.; Qi, S. L.; Harris, A. C.; Dennehy, K. F.; McMahon, P. B.; Degnan, J. R.; Böhlke, J. K. Brackish Groundwater in the United States. *Professional Paper; USGS Numbered Series 1833*; U.S. Geological Survey: Reston, VA, 2017; Vol. *1833*, p 202.
(33) Subramani, A.; Jacangelo, J. G. Emerging Desalination Technologies for Water Treatment: A Critical Review. *Water Res.* **2015**, *75*, 164−187.
(34) Gude, V. G. Desalination and Water Reuse to Address Global Water Scarcity. *Rev. Environ. Sci. Biotechnol.* **2017**, *16*, 591−609.
(35) Miyoshi, H. Diffusion Coefficients of Ions through Ion-Exchange Membranes for Donnan Dialysis Using Ions of the Same Valence. *Chem. Eng. Sci.* **1997**, *52*, 1087−1096.
(36) Agarwal, C.; Chaudhury, S.; Pandey, A. K.; Goswami, A. Kinetic Aspects of Donnan Dialysis through Nafion-117 Membrane. *J. Membr. Sci.* **2012**, *415−416*, 681−685.
(37) Hasson, D.; Beck, A.; Fingerman, F.; Tachman, C.; Shemer, H.; Semiat, R. Simple Model for Characterizing a Donnan Dialysis Process. *Ind. Eng. Chem. Res.* **2014**, *53*, 6094−6102.
(38) Ring, S.; Hasson, D.; Shemer, H.; Semiat, R. Simple Modeling of Donnan Separation Processes. *J. Membr. Sci.* **2015**, *476*, 348−355.
(39) Güler, E.; Elizen, R.; Vermaas, D. A.; Saakes, M.; Nijmeijer, K. Performance-Determining Membrane Properties in Reverse Electrodialysis. *J. Membr. Sci.* **2013**, *446*, 266−276.
(40) Fan, H.; Huang, Y.; Billinge, I. H.; Bannon, S. M.; Geise, G. M.; Yip, N. Y. Counterion Mobility in Ion-Exchange Membranes: Spatial Effect and Valency-Dependent Electrostatic Interaction. *ACS EST Eng.* **2022**, DOI: 10.1021/acsestengg.1c00457.
(41) Todd, D. K.; Mays, L. W. *Groundwater Hydrology*; John Wiley & Sons, 2004.

(42) Dieter, C. A.; Maupin, M. A.; Caldwell, R. R.; Harris, M. A.; Ivahnenko, T. I.; Lovelace, J. K.; Barber, N. L.; Linsey, K. S. Estimated Use of Water in the United States in 2015. *Circular; USGS Numbered Series 1441*; U.S. Geological Survey: Reston, VA, 2018; Vol. *1441*, p 76.
(43) *Guidelines for Drinking-Water Quality: Fourth Edition Incorporating the First Addendum; WHO Guidelines Approved by the Guidelines Review Committee*; World Health Organization: Geneva, 2017.
(44) Davis, T. A. Membrane Separations|Donnan Dialysis. In *Encyclopedia of Separation Science*; Wilson, I. D., Ed.; Academic Press: Oxford, 2000; pp 1701−1707.
(45) Yeh, H. M.; Chang, Y. H. Mass Transfer for Dialysis through Parallel-Flow Double-Pass Rectangular Membrane Modules. *J. Membr. Sci.* **2005**, *260*, 1−9.
(46) Yip, N. Y.; Elimelech, M. Thermodynamic and Energy Efficiency Analysis of Power Generation from Natural Salinity Gradients by Pressure Retarded Osmosis. *Environ. Sci. Technol.* **2012**, *46*, 5230−5239.
(47) Morel, F. M. M.; Hering, J. G. *Principles and Applications of Aquatic Chemistry*; John Wiley & Sons, 1993.
(48) Seader, J. D.; Henley, E. J.; Roper, D. K. *Separation Process Principles*; Wiley: New York, 1998; Vol. *25*.
(49) Fan, H.; Yip, N. Y. Elucidating Conductivity-Permselectivity Tradeoffs in Electrodialysis and Reverse Electrodialysis by Structure-Property Analysis of Ion-Exchange Membranes. *J. Membr. Sci.* **2019**, *573*, 668−681.
(50) Phuntsho, S.; Shon, H. K.; Hong, S.; Lee, S.; Vigneswaran, S. A Novel Low Energy Fertilizer Driven Forward Osmosis Desalination for Direct Fertigation: Evaluating the Performance of Fertilizer Draw Solutions. *J. Membr. Sci.* **2011**, *375*, 172−181.
(51) Phuntsho, S.; Hong, S.; Elimelech, M.; Shon, H. K. Forward Osmosis Desalination of Brackish Groundwater: Meeting Water Quality Requirements for Fertigation by Integrating Nanofiltration. *J. Membr. Sci.* **2013**, *436*, 1−15.
(52) Richa, A.; Touil, S.; Fizir, M.; Martinez, V. Recent Advances and Perspectives in the Treatment of Hydroponic Wastewater: A Review. *Rev. Environ. Sci. Biotechnol.* **2020**, *19*, 945−966.
(53) Stone, M. L.; Rae, C.; Stewart, F. F.; Wilson, A. D. Switchable Polarity Solvents as Draw Solutes for Forward Osmosis. *Desalination* **2013**, *312*, 124−129.
(54) Park, J.; Joo, H.; Noh, M.; Namkoong, Y.; Lee, S.; Jung, K. H.; Ahn, H. R.; Kim, S.; Lee, J.-C.; Yoon, J. H.; Lee, Y. Systematic Structure Control of Ammonium Iodide Salts as Feasible UCST-Type Forward Osmosis Draw Solutes for the Treatment of Wastewater. *J. Mater. Chem. A* **2018**, *6*, 1255−1265.

https://doi.org/10.1021/acsestengg.2c00152
ACS EST Engg. 2022, 2, 2076−2085